ACS Chemical Neuroscience

UNIVERSITY OF TECHNOLOGY SYDNEY

Subscriber access provided by UNIVERSITY OF TECHNOLOGY SYDNEY

Article

Synthesis and Preclinical Evaluation of an 18F-Labeled Synaptic Vesicle Glycoprotein 2A PET Imaging Probe: [18F]SynVesT-2

Zhengxin Cai, Songye Li, Wenjie Zhang, Richard Pracitto, Xiaoai Wu, Evan Baum, Sjoerd J. Finnema, Daniel Holden, Takuya Toyonaga, Shu-fei Lin, Marcel Lindemann, Anupama Shirali, David C. Labaree, Jim Ropchan, Nabeel Nabulsi, Richard E. Carson, and Yiyun Huang

ACS Chem. Neurosci., **Just Accepted Manuscript** • DOI: 10.1021/acschemneuro.9b00618 • Publication Date (Web): 21 Jan 2020

Just Accepted

is published by the American Chemical Society. 1155 Sixteenth Street N.W., Washington, DC 20036

Synthesis and Preclinical Evaluation of an ^{18}F-Labeled Synaptic Vesicle Glycoprotein 2A PET Imaging Probe: [^{18}F]SynVesT-2

Zhengxin Cai,[*,†] Songye Li,[*,†] Wenjie Zhang,[†,‡] Richard Pracitto,[†] Xiaoai Wu,[†,‡] Evan Baum,[†,&] Sjoerd J. Finnema,[†,′] Daniel Holden,[†] Takuya Toyonaga[†], Shu-fei Lin,[†] Marcel Lindemann,[†] Anupama Shirali,[†] David C. Labaree,[†] Jim Ropchan,[†] Nabeel Nabulsi,[†] Richard E. Carson,[†] Yiyun Huang[†]

[†]PET Center, Department of Radiology and Biomedical Imaging, Yale University, New Haven, CT 06520, USA.

[‡]Department of Nuclear Medicine, Laboratory of Clinical Nuclear Medicine, West China Hospital, Sichuan University, Chengdu, Sichuan 610041, China.

Supporting Information Placeholder

ABSTRACT: Synaptic vesicle glycoprotein 2A (SV2A) is a 12-pass transmembrane glycoprotein ubiquitously expressed in presynaptic vesicles. *In vivo* imaging of SV2A using PET has potential applications in the diagnosis and prognosis of a variety of neuropsychiatric diseases, *e.g.*, Alzheimer's disease, Parkinson's disease, schizophrenia, multiple sclerosis, autism, epilepsy, stroke, traumatic brain injury, post-traumatic stress disorder, depression, *etc*. Herein, we report the synthesis and evaluation of a new ^{18}F-labeled SV2A PET imaging probe, [^{18}F]SynVesT-2, which possesses fast *in vivo* binding kinetics and high specific binding signals in nonhuman primate brain.

KEYWORDS: SV2A, PET, nonhuman primate, Alzheimer's disease, Parkinson's disease, fluorine-18.

INTRODUCTION

Synaptic vesicle glycoprotein 2A (SV2A) is an essential presynaptic transmembrane protein[1]. SV2A is critical for neural system functioning[2, 3], and is dysregulated in epilepsy[4-7]. SV2A is also the binding target of the antiepileptic drug, levetiracetam (Keppra®)[8], which has been shown to improve cognitive function in patients with amnestic mild cognitive impairment (aMCI) and rodent models of memory loss and Alzheimer's disease (AD)[7, 9, 10], probably through regulation of mitochondrial function[11]. Positron emission tomography (PET) is a non-invasive quantitative imaging modality that provides functional information in living systems, and SV2A-targeted PET imaging may provide potentially prognostic information and elucidate the etiology and progression of a variety of neuropsychological diseases[12].

Several radioligands have been developed for imaging SV2A (**Figure 1**), including [^{11}C]levetiracetam (**1**)[13], [^{11}C]UCB-A (**2**)[14], [^{18}F]UCB-H (**3**)[15-18], [^{11}C]UCB-J (**4**)[19-22], [^{18}F]UCB-J (**5**)[23], and [^{18}F]SDM-8/[^{18}F]MNI-1126/[^{18}F]SynVesT-1[12, 24-26] (**6**). Among them, [^{11}C]UCB-J (**4**) has proved to be an excellent PET probe to image and quantify synaptic density in living brain[20], and has been applied to the studies of a variety of neurodegenerative and neuropsychiatric disorders[22, 27, 28]. However, the use of [^{11}C]UCB-J requires an on-site cyclotron, and its accessibility as a clinical research tool is limited due to the short half-life of ^{11}C (20.38 minutes). Thus, we set out to develop the ^{18}F-labeled counterpart, [^{18}F]UCB-J[23, 29], while exploring the chemical space around the common pyrrolidinone pharmacophore, and synthesized analogs of UCB-J that are readily radiofluorinated using recently developed radiofluorination methods[30-37]. Among the newly synthesized analogs, we identified [^{18}F]SDM-8/[^{18}F]SynVesT-1 (**6**)[24, 38] and [^{18}F]SDM-2/[^{18}F]SynVesT-2 ([^{18}F]**7**)[39] as ^{18}F-labeled candidate SV2A imaging probes with optimal imaging characteristics. Radioligand **6** was initially synthesized by us and Invicro independently, and given different names (SDM-8 by Yale, MNI-1126 by Invicro). To avoid future confusion in reference to the radioligand, we and the Invicro group agreed to use SynVesT-1 (Synaptic Vesicle Tracer-1) to refer to this radioligand. Accordingly, SDM-2 will be referred to as SynVesT-2 in future publications. Herein, we report the synthesis and preliminary evaluations of [^{18}F]**7** in nonhuman primates.

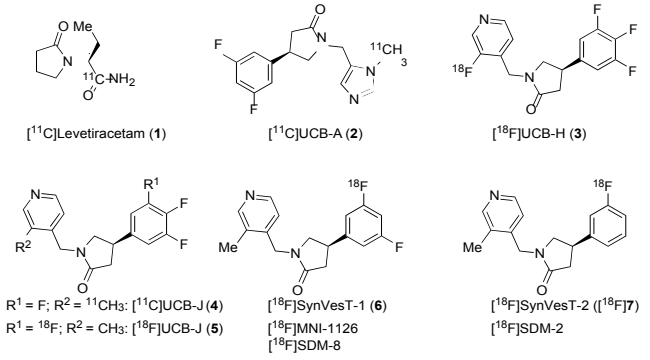

Figure 1. Current SV2A radioligands.

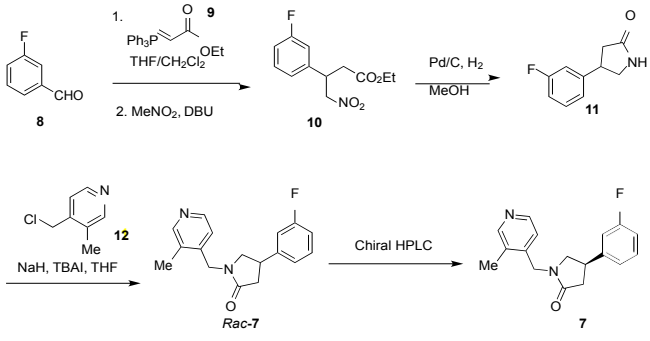

Scheme 1. Synthesis of the standard compound for [^{18}F]SDM-2/[^{18}F]SynVesT-2 ([^{18}F]**7**).

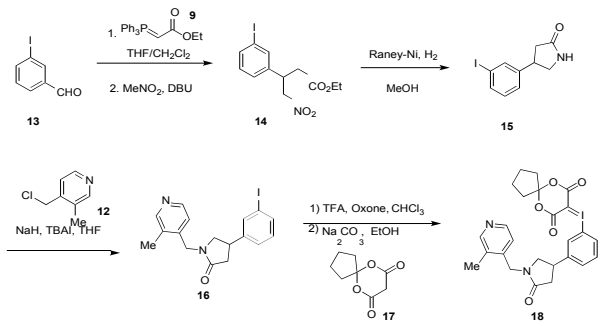

Scheme 2. Synthesis of the iodonium ylide precursor (**18**).

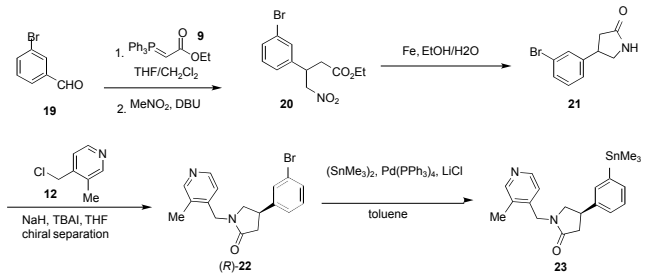

Scheme 3. Synthesis of the organostannane precursor (**23**).

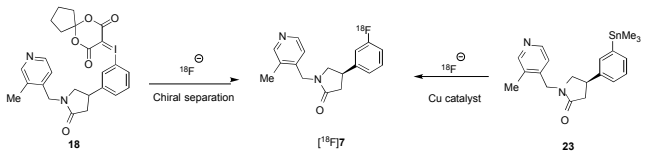

Scheme 4. Radiosynthesis of [^{18}F]SDM-2/[^{18}F]SynVesT-2 ([^{18}F]**7**) via the iodonium ylide precursor (**18**) or organostannane precursor (**23**).

RESULTS AND DISCUSSION

Chemistry. As radiofluorination of UCB-J was shown to be challenging, we decided to modify the structure of UCB-J to allow for efficient radiofluorination using existing methodologies without compromising the binding affinity to SV2A. The structural modifications also provided us with the opportunity to study the structure-pharmacokinetics (PK) relationship of this series of SV2A ligands. Compared with UCB-J, its monofluorinated analogs possess attractive characteristics as being amenable for radiofluorination, less lipophilic, and potentially less nonspecific binding *in vivo*. Because even subtle structural changes of small organic molecules could lead to dramatic changes in binding affinity, *in vivo* stability and PK profile, we synthesized and screened a library of monofluorinated analogs and found that compound **7** possessed the highest binding affinity[39]. Analog **7** was synthesized starting from a Wittig reaction using commercially available 3-fluorobenzaldehyde (**8**) and (carbethoxymethylene)triphenylphosphorane (**9**), followed by treatment with nitromethane under basic conditions to give compound **10**, which was reduced and cyclized to yield pyrrolidinone **11**. *N*-alkylation of **11** with 4-(chloromethyl)-3-methylpyridine (**12**) generated racemic **7** in 78% yield (**Scheme 1**). The enantiopure compound **7** and its enantiomer were isolated after chiral HPLC separation. The *in vitro* binding affinity of **7** was then tested through competition binding assays with [^{3}H]UCB-J in rat and human brain tissue homogenates[40]. The K_i values of **7** were 7.6 nM and 12 nM for rat and human SV2A respectively; while the K_i values of its enantiomer, the (*S*)-**7**, were 18 nM and 71 nM for rat and human SV2A, respectively[40]. Although the K_i values of **7** were higher than those of UCB-J (K_i: 3.5 nM and 1.5 nM for rat and human SV2A)[40] and SynVesT-1 (K_i: 2.0 nM and 4.7 nM for rat and human SV2A)[40], **7** still holds promise as a suitable PET tracer candidate for brain SV2A imaging, because of the high B_{max} of SV2A in the brain. Assuming the protein content in the brain tissue is 10% and tissue density is 1 g/mL, the B_{max} values are 4.5 pmol/mg protein[41] (450 nM) and 3-4 pmol/mg protein[41] (300-400 nM) in rat and human brains, respectively.

As the synthesis of [^{18}F]**7** involved the radiofluorination of an unactivated aromatic ring[37,43], we reasoned that hypervalent iodonium precursors, *i.e.*, diaryliodonium salts[32] and iodonium ylides[34, 44-48], and organostannane precursors[36] would be suitable for the radiosynthesis of [^{18}F]**7**. Thus, we synthesized both the iodonium ylide and organostannane precursors. Synthesis of the iodonium ylide precursor (**Scheme 2**) started with a Wittig reaction using **13** and **9**, followed by Michael addition, Raney-Ni-catalyzed reduction, and cyclization, yielding pyrrolidinone **15** in 30% yield over four steps. *N*-alkylation of **15** with **12** generated **16** in 68% yield. The iodonium ylide **18** was prepared in 30% yield by oxidation of the iodide **16** with Oxone, followed by reaction with 6,10-dioxaspiro[4.5]decane-7,9-dione (**17**). Next, we tested the radiolabeling conditions by heating **18** in *N,N*-dimethylformamide (DMF) with [^{18}F]Et_4NF and Et_4NHCO_3 at 150 °C for 10 min, and obtained the formulated [^{18}F]**7** in less than 1% radiochemical yield (RCY), after a reverse phase HPLC purification and a chiral HPLC separation, with molar activity of 857 ± 770 MBq/nmol (n = 9) at the end of synthesis (EOS) (**Table S1**). Lower radiochemical conversions were observed at lower radiolabeling temperatures, based on the radio-HPLC analysis of the crude reaction mixture.

We then explored the radiofluorination using an organostannane precursor, which was synthesized following the same synthetic route as **18**. Starting with 3-bromobenzaldehyde (**19**), the bromide (±)-**22** was synthesized in 67% yield over five steps (**Scheme 3**). After separation of the two enantiomers of **22**, enantiopure organostannane (*R*)-**23** was prepared in 59% yield via palladium-catalyzed stannylation (**Scheme 3**). Radiofluorination of **23** was carried out in *N,N*-dimethylacetamide (DMA) at 110 °C for 20 min in the presence of [^{18}F]KF, copper(II) triflate, and pyridine to give [^{18}F]**7** in an average radiochemical yield of 6.8% (n = 9, decay corrected) after semipreparative HPLC (**Figure 2A**), with an average molar activity of 141 MBq/nmol (n=8) at EOS (**Table S2**). The accrued synthesis, purification, and formulation time was less than 90 min. The radiochemical purity of [^{18}F]**7** was greater than 99% and [^{18}F]**7** coeluted with **7** under the same HPLC conditions (**Figure 2B**). No racemization of the product was observed under these radiolabeling conditions (**Figure 2C**). And the final product in the formulated solution was tested to be stable for at least 4 h at room temperature.

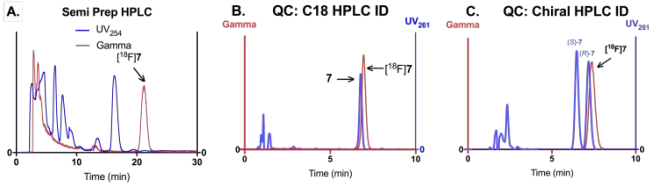

Figure 2. Representative HPLC chromatograms of [^{18}F]**7** as in the crude reaction mixture (A), co-injected with the standard compound **7** on a Luna C18 (5μm, 4.6 × 250 mm) column (B), and co-injected with the racemic **7** on a ChiralCel ODRH (5 μm, 4.6 × 150 mm) column, eluting with a mobile phase (pH 4.2) of 35% CH_3CN and 65% 0.1 M ammonium formate solution with

0.5% acetic acid at a flow rate of 1 mL/min (C). The red indicates gamma peaks; the blue indicates UV peaks.

***In Vitro* Study**. The partition coefficient log*D* was determined by the ratio of decay-corrected radioactivity concentrations in *n*-octanol and PBS. Log*D* of [^{18}F]**7** is 2.17 ± 0.02 (n = 3), which is within the optimal range for blood-brain barrier penetration[49], and is lower than those of **4** and **6** (Log*D*: 2.53 and 2.32 for **4** and **6**, respectively).

PET Imaging in Nonhuman Primates. The injected activity ranged from 163.7 to 185.9 MBq (n = 4), corresponding to 23.3 – 57.6 ng of **7**. The plasma free fraction (f_P) of [^{18}F]**7** was 41 ± 2% (n = 3), which is slightly lower than that of **4** (46.2 ± 2.5%, n = 11). The total radioactivity in the plasma showed a sharp increase within three minutes, a fast washout phase, followed by a slow washout phase (**Figure 3A**). The metabolism rate of [^{18}F]**7** was moderate and similar to that of **4**, with 34 ± 0.1% of intact parent radiotracer at 30 min post-injection (*p.i.*), which further decreased to 24 ± 3% and 22 ± 4%, at 60 and 90 min respectively (**Figure 3B**). The radioactive metabolites in the plasma were shown to have shorter retention times than the parent compound on the HPLC chromatogram, indicating that they were more hydrophilic and less likely to penetrate the BBB (**Figure 3C**).

High quality brain PET images were generated with [^{18}F]**7** in rhesus monkey, with high tracer uptake in grey matter and very low uptake in white matter (**Figure 4A**). The tracer entered brain quickly after intravenous injection, with peak standardized uptake value (SUV) around 8.5 within 10 min *p.i.* (**Figure 4B**). We observed higher tracer uptake in the frontal cortex and putamen (peak SUV > 8), and lowest uptake in the white matter region, *i.e.*, centrum semiovale (SUV < 2). [^{18}F]**7** displayed faster kinetics than **4 and 6 (Figure S1)**, reaching apparent equilibrium within 60 min *p.i.* in most brain regions (**Figure 4C**). No tracer uptake in skull was observed even from the late PET images, indicating the lack of *in vivo* defluorination. When the animal was pretreated with UCB-J (150 µg/kg, *i.v.*), the whole brain SUV decreased to the same level as centrum semiovale, indicating the *in vivo* binding specificity of [^{18}F]**7** to SV2A (**Figure 4D**).

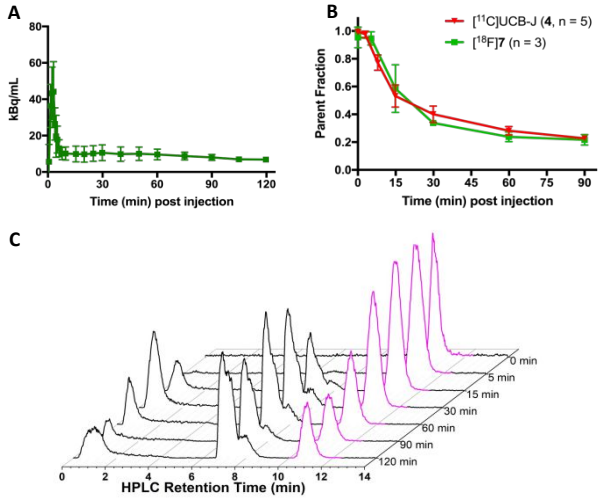

Figure 3. (A) Total plasma radioactivity (kBq/mL) over time. (B) Unmetabolized parent fraction of [^{18}F]**7** (in green) and **4** (in red) from baseline nonhuman primate PET scans. (C) Radio-HPLC chromatograms of plasma metabolite analysis of [^{18}F]**7** (retention time at 11 min) over time. Organic contents captured on a short C18 column were backflushed onto a Phenomenex Luna C18(2) column (5μm, 4.6 × 250 mm) eluting with 37% acetonitrile/63% 0.1 M ammonium formate (pH6.4) at flow rate of 2 mL/min.

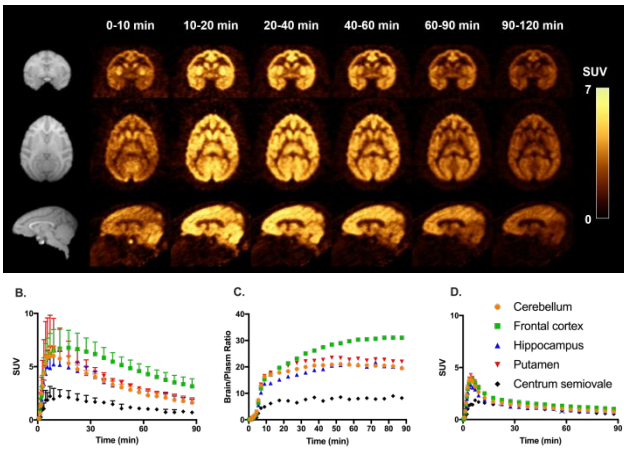

Figure 4. (A) Summed SUV images of [^{18}F]SynVesT-2 ([^{18}F]**7**) in the brain of a rhesus monkey from different imaging windows. (B) Regional time-activity curves (TACs) of [^{18}F]**7** from baseline PET scans (n = 3). (C) Time course of regional tracer uptake to arterial input ratios. (D) TACs of pre-blocking scan with pre-injected UCB-J (150 µg/kg, *i.v.*, n = 1).

Table 1. Distribution volumes (V_T/mL·cm^{-3})* of **4**, **6**, **7**, and **7** with pre-blocking in monkey brain regions calculated with 1TCM.

Radiotracer	[^{18}F]Syn-VesT-2 **(7)**	[^{11}C]UCB-J **(4)**	[^{18}F]Syn-VesT-1 **(6)**	[^{18}F]Syn-VesT-2 **(7)**
Brain regions	n = 3	n = 6	n = 3	Preblocking
Cingulate cortex	18.2 ± 2.2	55.6 ± 10	48.5 ± 8.9	5.34
Frontal cortex	17.5 ± 2.2	55.4 ± 8.2	47.1 ± 9.1	4.9
Nucleus accumbens	16.9 ± 2.7	54 ± 9.2	45.2 ± 7.9	4.82
Insular cortex	16.4 ± 2.9	54.6 ± 6.7	46.1 ± 9.2	4.72
Occipital cortex	15.7 ± 2.8	52.9 ± 7.1	43.7 ± 10.7	4.53
Temporal cortex	14.7 ± 2.6	50.5 ± 6.9	42.2 ± 10.0	4.31
Caudate nucleus	13.6 ± 2.3	44.9 ± 4.6	35.0± 6.3	4.36
Thalamus	13.3 ± 2.6	40.3 ± 6.5	34.2 ± 3.0	3.82
Putamen	13.2 ± 2.2	45.2 ± 3.1	34.6 ± 4.9	4.35
Hippocampus	10.9 ± 2.7	34.5 ± 2.8	30.1 ± 5.6	3.47
Cerebellum	10.8 ± 2.8	36± 5.3	28.9 ± 6.8	3.79
Globus pallidus	8.8 ± 1.9	28 ± 3	21.6 ± 4.2	4.01
Amygdala	8.8 ± 2.5	24.8 ± 1.9	24.8± 8.5	2.63
Brainstem	6.6 ± 3	23.6 ± 2.9	16.3± 3.6	3.1
Pons	6.5 ± 3.5	23.4 ± 3.2	16.0± 3.4	3.08
Centrum semiovale	4.4 ± 1.6	13.6 ± 2.9	8.9± 2.0	3.19

*Data are single or multiple (n) measurements represented as single value or mean ± SD, respectively. SD is standard deviation. Pre-blocking scan was done with pre-injected UCB-J (150 µg/kg, n = 1).

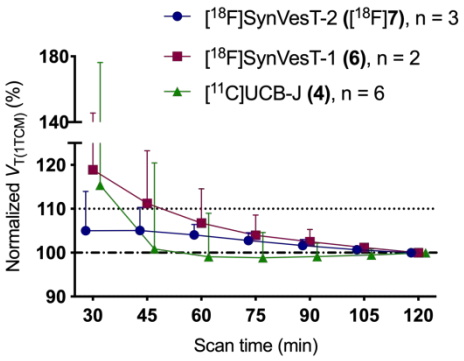

Figure 5. Time stability of V_T estimates (1TCM) of **4**, **6**, and [^{18}F]**7** in 17 brain regions of nonhuman primates. The V_T values estimated using scan durations ranging from 30 to 120 min were analysed in 15 min increments. The y-axis represents percentage of V_T value derived from 120 min scan datasets.

Kinetic Modelling. For [^{18}F]**7**, the 1-tissue compartment model (1TCM) produced suitable fits and reliable estimates of regional distribution volume (V_T), the equilibrium ratio of brain to plasma. The V_T values ranged from 4.4 ± 1.6 (n = 3) for centrum semiovale to 18.2 ± 2.2 (n = 3) for cingulate cortex, and were globally lower than those of [^{11}C]UCB-J (**4**) (**Table 1**). Note that [^{18}F]**7** has lower uptake than [^{11}C]UCBJ (**4**) and [^{18}F]SDM-8/SynVesT-1 (**6**) in the centrum semiovale, which is considered a region with mainly non-specific binding and could be used as reference region for noninvasive quantitative data analysis[50]. The lower V_T values of [^{18}F]**7** in centrum semiovale (4.4 ± 1.6 V_T/mL·cm^{-3}, compared with 13.6 ± 2.9 V_T/mL·cm^{-3} and 8.9 ± 2.0 V_T/mL·cm^{-3} for **4** and **6**, respectively) (**Table 1**) is consistent with its slightly lower log*D* value (2.17, compared with 2.53 and 2.32 for **4** and **6**, respectively).

Table 2. Binding potential (BP_{ND}) values* of **4**, **6**, **7**, and **7** with pre-blocking in monkey brain regions calculated from the V_T values using centrum semiovale as reference region.

Radiotracer	[^{18}F]SynVesT-2 **(7)**	[^{11}C]UCB-J **(4)**	[^{18}F]SynVesT-1 **(6)**	[^{18}F]SynVesT-2 **(7)**
Brain regions	n = 3	n = 6	n = 3	Preblocking
Cingulate cortex	3.5 ± 1.6	3.2 ± 0.9	4.5 ± 0.4	0.68
Frontal cortex	3.3 ± 1.5	3.2 ± 1	4.3 ± 0.6	0.54
Nucleus accumbens	3.2 ± 1.3	3.1 ± 0.7	4.1 ± 0.4	0.48
Insular cortex	3 ± 1.3	3.2 ± 0.9	4.2 ± 0.3	0.51
Occipital cortex	3 ± 1.5	3 ± 0.7	3.9 ± 0.2	0.42
Temporal cortex	2.7 ± 1.4	2.8 ± 0.7	3.7 ± 0.3	0.35
Caudate nucleus	2.3 ± 0.9	2.4 ± 0.8	3.0 ± 0.4	0.36
Putamen	2.3 ± 0.9	2.5 ± 0.7	2.9 ± 0.4	0.37
Thalamus	2.2 ± 0.8	2.1 ± 0.7	2.9 ± 0.7	0.20
Cerebellum	1.6 ± 0.8	1.7 ± 0.4	2.2 ± 0.2	0.19
Hippocampus	1.6 ± 0.6	1.6 ± 0.4	2.4 ± 0.4	0.09
Globus pallidus	1.2 ± 0.7	1.1 ± 0.3	1.4 ± 0.3	0.26
Amygdala	1.1 ± 0.3	0.9 ± 0.4	1.9 ± 1.1	-0.18
Brainstem	0.6 ± 0.5	0.8 ± 0.3	0.8 ± 0.0	-0.03
Pons	0.5 ± 0.6	0.8 ± 0.3	0.8 ± 0.0	-0.03

*Data are single or multiple (n) measurements represented as single value or mean ± SD, respectively. SD is standard deviation. Pre-blocking scan was done with pre-injected UCB-J (150 μg/kg, n = 1).

PET tracer with faster pharmacokinetics are expected to reach equilibrium more quickly, and needs shorter scan time for reliable V_T estimation. Thus, we evaluated the time stability of the V_T estimation (1TCM) for 17 brain regions, by choosing different scan durations for 1-tissue compartmental modelling, and compared the minimum scan times required by [^{18}F]**7**, **4**, and **6**. As expected, a 30-min scan time was needed for [^{18}F]**7** to generate reliable V_T estimates (averaged V_T values within 10% deviation from the 120-min V_T values); while 45 min and 60 min scan durations were needed for **4** and **6**, respectively (**Figure 5**). As early imaging provides K_1 map, reflecting brain perfusion[22], dynamic scans using [^{18}F]**7** could provide information on both cerebral blood flow and SV2A binding in shorter scan time than that required for **4** and **6**.

The specific binding signals, as presented by the regional non-displaceable binding potential (BP_{ND}) values, were highly similar to those of [^{11}C]UCB-J (**4**) (**Table 2**), due to the lower nonspecific binding as evidenced by the lower uptake of [^{18}F]**7** in the white matter, which was used as the reference region in BP_{ND} calculation. The BP_{ND} value was highest in the cingulate cortex, followed by the frontal cortex, nucleus accumbens, insula, occipital, temporal cortex, caudate putamen, thalamus, cerebellum, hippocampus, globus pallidus, amygdala, and brainstem, consistent with the regional distribution of SV2A[19, 20]. Due to partial volume effect in the sentrum semiovale of nonhuman primates, the BP_{ND} calculated using sentrum semiovale could be biased. The issue of using centrum semiovale as reference for quantitative data analysis has been studied by several groups[50-52].

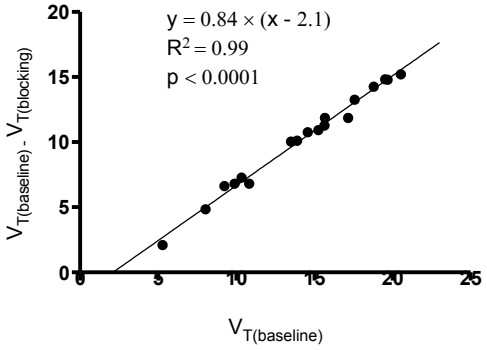

Figure 6. Receptor occupancy plot (Lassen plot) of the difference between the V_T values of [^{18}F]**7** with and without pre-injected UCB-J (150 μg/kg, *i.v.*) against the baseline V_T values in the same rhesus monkey. The slope of the linear regression is the estimated SV2A occupancy by UCB-J (150 μg/kg, *i.v.*), and the x-intercept is the estimated nondisplaceable volume of distribution (V_{ND}).

Based on Lassen plot analysis, the SV2A-specific ligand UCB-J (150 μg/kg, preinjected intravenously) blocked 84% of tracer binding, indicating high *in vivo* binding specificity of [^{18}F]**7** (**Figure 6**). The non-displaceable volume of distribution (V_{ND}) of [^{18}F]**7** calculated from Lassen plot was 2.1 mL/cm^3, which was lower than the V_{ND} of **4** (6.27 mL/cm^3), and **6** (2.97 mL/cm^3). Under the same blocking condition, similar SV2A occupancy was achieved when **4** (87%) or **6** (79%, **Figure S3**) was used as the PET ligand[19].

CONCLUSIONS. In summary, we evaluated a new ^{18}F-labeled SV2A PET imaging probe, [^{18}F]**7**, which was synthesized via iodonium ylide and organostannane precursors in high molar activity and high radiochemical purity. PET imaging in monkeys demonstrated that the new SV2A radioligand [^{18}F]**7** exhibited excellent image quality and suitable pharmacokinetics for quantitative kinetic modelling and provided specific binding signals highly similar to those of [^{11}C]UCB-J (**4**) in nonhuman primates using white matter as reference region, but with faster kinetics, which could be advantageous in the clinical setting. The synthesis

process using the organostannane precursor (**23**) has been validated for production of [^{18}F]**7** for human use. Translation of [^{18}F]**7** into human evaluation is underway at Yale PET Center and will be reported in due course.

METHODS

Chemistry. *Materials, Instruments, and General Methods.* All reagents and solvents were obtained from commercial sources (Sigma-Aldrich, TCI, and Fisher Scientific) and used without further purification unless noted otherwise. Nuclear magnetic resonance (^{1}H-, ^{13}C-, and ^{19}F-NMR) spectra were recorded on an Agilent DD2 400 MHz (A400a), Agilent DD2 500 MHz (A500a), Varian 400 MHz, or AVANCE III 400 MHz UltraShield-Plus Digital NMR Spectrometer. Chemical shifts are reported in parts per million, with the solvent resonance as the internal standard ($CDCl_3$: 7.26 ppm; DMSO-d_6: 2.49 ppm). Melting point was examined on an Electrothermal Mel-Temp instrument. High-performance liquid chromatography-mass spectrometry (HPLC-MS) was performed with an Agilent 1200RRLC/6110SQD system. High resolution mass spectrometry (HRMS) was done with Thermo LTQ Orbitrap spectrometer. [^{18}F]Fluoride was produced via the ^{18}O(p, n) ^{18}F nuclear reaction in a 16.5-MeV GE PETtrace cyclotron (Uppsala, Sweden). $H_2{}^{18}O$ was obtained from Huayi Isotopes (Toronto, Canada). Anion exchange Chromafix cartridges (PS-HCO_3) were purchased from Macherey-Nagel (Dueringen, Germany). Solid-phase extraction (SPE) cartridges were purchased from Waters Associates (Milford, MA, USA). All chemicals used in this study were of ≥ 95% purity, based on HPLC, LC-MS, or NMR analysis. The semi-preparative HPLC system comprises a Shimadzu LC-20A pump, a Knauer K200 UV detector, and a Bioscan γ-flow detector, with a Luna C18(2) column (10 × 250 mm, 10 μm, Phenomenex, Torrance, CA, USA). The chiral semi-preparative HPLC system uses a ChiralCel OD-H column (10 × 250 mm, 5 μm, ChiralCel, West Chester, PA, USA). For quality control, we used a Shimadzu LC-20A pump, a Shimadzu SPD-M20A PDA or SPD-20A UV detector, a Bioscan γ-flow detector, with a Genesis C18 column (4.6 × 250 mm, 4 μm, Hichrom, Berkshire, UK) eluting with a mobile phase (pH 4.2) of 34% CH_3CN and 66% 0.1 M ammonium formate solution with 0.5% acetic acid at a flow rate of 2 mL/min for purity check as well as a ChiralCel OD-RH (4.6 × 150 mm, 5 μm, ChiralCel, West Chester, PA, USA) eluting with a mobile phase (pH 4.2) of 30% CH_3CN and 70% 0.1 M ammonium formate solution with 0.5% acetic acid at a flow rate of 1 mL/min or a mobile phase (pH 4.2) of 35% CH_3CN and 65% 0.1 M ammonium formate solution with 0.5% acetic acid at a flow rate of 1 mL/min. Chemical identity of the tracer was confirmed by co-elution of the tracer co-injected with its non-radioactive (*R*)-**7**.

Ethyl 3-(3-fluorophenyl)-4-nitrobutanoate (10): 3-Fluorobenzaldehyde (**8**, 4 g, 32.3 mmol) was dissolved in anhydrous THF (8 mL) in an oven-dried round bottom flask and the solution cooled on ice to ca. 5 °C. The solution of carbethoxymethylene triphenyl phosphorene (**9**, 11.8 g, 33.9 mmol) in anhydrous CH_2Cl_2 (25 mL) was then added dropwise at 5 °C. The reaction mixture was stirred for 30 min at 5 °C, and concentrated to dryness *in vacuo*. A mixture of *n*-hexanes and Et_2O (200 mL, 10:1, *v*/*v*) was added to the white residue and the suspension stirred for 30 min at ambient temperature. The solid was filtered and the filtrate evaporated to yield a white solid (6.5 g), which was dissolved in nitromethane (4 mL, 74.8 mmol) and cooled on ice to 5 °C. 1,8-Diazabicyclo(5.4.0)undec-7-ene (DBU, 4.39 g, 28.9 mmol) was then added dropwise and the solution stirred for 1 h at 5 °C. The reaction was quenched with saturated NH_4Cl solution (50 mL), acidified with aqueous HCl (2 M), and extracted with EtOAc (50 mL × 3). The combined organic phases were washed with brine (100 mL), dried with Na_2SO_4, and concentrated *in vacuo* to give **9** as a yellow oil (5.7 g, 77%), which was used in the next step of synthesis without further purification. ^{1}H NMR ($CDCl_3$, 400 MHz): δ 7.39 – 7.21 (m, 1H), 7.11 – 6.90 (m, 3H), 4.73 (dd, J = 12.8, 6.7 Hz, 1H), 4.63 (dd, J = 12.7, 8.2 Hz, 1H), 4.20 – 4.04 (m, 2H), 4.04 – 3.83 (m, 1H), 2.74 (dd, J = 7.4, 2.4 Hz, 2H), 1.18 (t, J = 7.1 Hz, 3H).

4-(3-Fluorophenyl)pyrrolidin-2-one (11): A solution of ethyl 3-(3-fluorophenyl)-4-nitrobutanoate (**10**, 0.56 g, 2.2 mmol) in MeOH (5 mL) was degassed with argon for 5 min, Pd/C (10%, 0.36 g) was added, and the suspension stirred under an atmosphere of hydrogen at ambient temperature for 12 h. The reaction mixture was filtered through a layer of Celite and the filtrate concentrated *in vacuo*. The crude product was purified by flash column chromatography on silica gel (0-10% EtOH/EtOAc) to provide **11** as a colorless oil (390 mg, 99%). ^{1}H NMR ($CDCl_3$, 400 MHz): δ 7.29 (q, J = 7.3, 6.89 Hz, 1H), 7.01 (d, J = 7.6 Hz, 1H), 6.94 (t, J = 8.2 Hz, 2H), 3.78 (t, J = 8.8 Hz, 1H), 3.68 (p, J = 8.2 Hz, 1H), 3.39 (t, J = 8.5 Hz, 1H), 2.73 (dd, J = 16.9, 8.9 Hz, 1H), 2.46 (dd, J = 16. 9, 8.6 Hz, 1H).

4-(3-Fluorophenyl)-1-((3-methylpyridin-4-yl)methyl)pyrrolidin-2-one (7): To an oven-dried vial cooled at 0 °C was added a solution of 4-(3-fluorophenyl)pyrrolidin-2-one (**11**) (55 mg, 0.31 mmol) in anhydrous THF (2.0 mL) and sodium hydride (61 mg, 1.54 mmol). The corresponding chloromethyl pyridine (**12**, 0.37 mmol) was then added and the mixture stirred overnight at ambient temperature. The reaction was quenched with saturated $NaHCO_3$ solution (6 mL) and extracted with EtOAc (3 mL × 3). The organic extracts were combined, dried over Na_2SO_4 and concentrated *in vacuo*. The crude product was purified with flash column chromatography on silica gel eluting with 0-10% EtOH/EtOAc to afford the racemic **7** (69 mg, 78%) as a light yellow oil. ^{1}H NMR ($CDCl_3$, 400 MHz): δ 8.40 (s, 2H), 7.29 (q, J = 7.4, 7.4 Hz, 1H), 7.03 (d, J = 4.8 Hz, 1H), 6.95 (d, J = 8.0 Hz, 2H), 6.88 (d, J = 10.0 Hz, 1H), 4.60 (d, J = 15.6 Hz, 1H), 4.40 (d, J = 15.5 Hz, 1H), 3.59 (m, 2H), 3.26 (m, 1H), 2.90 (dd, J = 17.1, 8.2 Hz, 1H), 2.62 (dd, J = 17.1, 7.6 Hz, 1H), 2.29 (s, 3H). ^{13}C NMR ($CDCl_3$, 100 MHz): δ 173.57, 151.05 (2C), 147.77 (2C), 142.96,131.65, 130.48 (split 2 peaks), 122.32 (split 2 peaks), 122.29, 114.15 (split 2 peaks), 113.71 (split 2 peaks), 53.76, 43.54, 38.21, 36.94, 15.93. ^{19}F NMR ($CDCl_3$, 376 MHz): δ -112.17. HRMS: calculated for $C_{17}H_{17}FN_2O$ $[M + H]^+$ 285.1398; found, 285.1393.

Chiral HPLC separation of 7: A solution of the racemic **7** (2 mg/mL, in *n*-hexane/EtOH, 70/30, *v*/*v*, with 0.1% Et_3N) was loaded on to a Daicel Chiralpak IA column (10 × 250 mm, 5 μm) and eluted with *n*-hexane/EtOH (70/30, *v*/*v*, with 0.1% Et_3N) at a flow rate of 4 mL/min. (*R*)-**7** was obtained after combination of collected fractions and evaporation of solvents under reduced pressure, with *ee*. > 98.6%. The stereochemistry assignment was based on analogy with the assignment of the two enantiomers of UCB-J on chiral HPLC eluting sequence, *i.e*., the first peak being (*S*), the second peak (*R*).

Ethyl 3-(3-iodophenyl)-4-nitrobutanoate (14): 3-Iodobenzaldehyde (**13**, 4 g, 17.2 mmol) was dissolved in anhydrous THF (10 mL) in an oven-dried round bottom flask and the solution was cooled in an ice bath to ca. 5 °C. A solution of carbethoxymethylene triphenyl phosphorene (6 g, 17.2 mmol) in anhydrous CH_2Cl_2 (20 mL) was then added dropwise at 5 °C. The reaction mixture was stirred for 30 min at 5 °C. When the reactants were completely consumed based on TLC analysis, the reaction mixture was evaporated *in vacuo* to near dryness. A mixture of hexanes and Et_2O (150 mL, 10:1, *v*/*v*) was added, and the suspension was stirred for 2 h at ambient temperature. The solution was filtered, and the filtrate was evaporated to dryness *in vacuo* to yield a white solid (4.5 g), which was dissolved in nitromethane (2.5

mL, 46.7 mmol) and cooled on ice to ca. 5 °C. Then, 1,8-diazabicyclo(5.4.0)undec-7-ene (DBU, 2.62 g, 17.2 mmol) was added dropwise, and the mixture was stirred at ca. 5 °C for 1 h. The reaction was quenched with saturated NH_4Cl solution (20 mL), and acidified with aqueous HCl (2 M). The mixture was extracted with EtOAc (25 mL × 3). The combined organic extracts were washed with brine (50 mL), dried with Na_2SO_4, filtered, and concentrated *in vacuo* to provide **14** as a yellow oil (6.7 g), which was used in the next step of synthesis without further purification. ^{1}H NMR ($CDCl_3$, 400 MHz): δ 7.70 – 7.53 (m, 2H), 7.22 (m, 1H), 7.07 (td, J = 7.7, 1.8 Hz, 1H), 4.82 – 4.68 (m, 1H), 4.68 – 4.57 (m, 1H), 4.18 – 4.01 (m, 2H), 4.01 – 3.84 (m, 1H), 2.73 (ddd, J = 7.7, 3.6, 1.6 Hz, 2H), 1.18 (td, J = 7.1, 2.0 Hz, 3H).

4-(3-Iodophenyl)pyrrolidin-2-one (15): A solution of ethyl 3-(3-iodo phenyl)-4-nitrobutanoate (**14**, 545 mg, 1.5 mmol) in EtOH (5 mL) was degassed with argon for 5 min. Raney-Ni (50% in water, 0.8 mL) was added in one portion. The suspension was then stirred under an atmosphere of hydrogen at ambient temperature for 2 days. The mixture was filtered through a layer of Celite and the filtrate concentrated *in vacuo*. The crude product was dissolved in toluene (50 mL), heated to reflux for 3 h, and concentrated *in vacuo*. The crude product was purified by flash column chromatography on silica gel (0-10% EtOH/EtOAc) to give **15** as a yellow oil (430 mg, 30%). ^{1}H NMR ($CDCl_3$, 400 MHz): δ 7.59 (d, J = 6.4 Hz, 2H), 7.21 (d, J = 7.7 Hz, 1H), 7.07 (t, J = 8.0 Hz, 1H), 5.99 (s, 1H), 3.76 (t, J = 8.8 Hz, 1H), 3.62 (p, J = 8.3 Hz, 1H), 3.38 (t, J = 7.4 Hz, 1H), 2.71 (dd, J = 16.9, 8.9 Hz, 1H), 2.44 (dd, J = 16.9, 8.6 Hz, 1H).

4-(3-Iodophenyl)-1-((3-methylpyridin-4-yl)methyl)pyrrolidin-2-one (16): To a solution of **15** (250 mg, 0.87 mmol) in anhydrous THF (3 mL) under argon and cooled at 0 °C was added sodium hydride (110 mg, 2.75 mmol). Tetrabutylammonium iodide (TBAI, 17 mg, 0.05 mmol) and 4-(chloromethyl)-3-methylpyridine hydrochloride (**11**, 180 mg, 0.96 mmol) were added after 30 min. The reaction mixture was kept stirring for 16 h at ambient temperature, then quenched with saturated $NaHCO_3$ solution (6 mL) and extracted with EtOAc (3 mL × 3). The organic extracts were combined, dried over Na_2SO_4 and concentrated *in vacuo*. The crude product was purified on a silica gel column eluting with 0-10 % EtOH/EtOAc to afford compound **16** as a light brown oil (256 mg, 68 %). ^{1}H NMR ($CDCl_3$, 400 MHz): δ 8.41 (s, 2H), 7.58 (dt, J = 7.8, 1.4 Hz, 1H), 7.51 (m, 1H), 7.13 (dt, J = 7.8, 1.4 Hz, 1H), 7.05 (d, J = 10.1 Hz, 1H), 7.03 (d, J = 7.5 Hz, 1H), 4.57 (d, J = 15.5 Hz, 1H), 4.42 (d, J = 15.5 Hz, 1H), 3.59 (m, 1H), 3.53 (p, J = 8.6 Hz, 1H), 3.23 (m, 1H), 2.88 (dd, J = 17.0, 8.8 Hz, 1H), 2.60 (dd, J = 17.0, 8.1 Hz, 1H), 2.30 (s, 3H).

8-((3-(1-((3-Methylpyridin-4-yl)methyl)-5-oxopyrrolidin-3-yl)phenyl)-λ^3-iodaneylidene)-6,10-dioxaspiro[4.5]decane-7,9-dione (**18**): To a solution of **16** (300 mg, 1.04 mmol) in $CHCl_3$ (1.5 mL) was added trifluoroacetic acid (TFA, 2.5 mL, 32.4 mmol) followed by Oxone (480 mg, 1.56 mmol). The reaction mixture was stirred for 2 h until it turned to a white suspension. The volatile contents were removed *in vacuo*. The residue was suspended in EtOH (2 mL) and 6,10-dioxaspiro[4.5]decane-7,9-dione (**17**, 220 mg, 1.29 mmol) was added, followed by 10% Na_2CO_3 until the pH of the mixture reached 10. The reaction mixture was stirred for 3 h, diluted with water, and extracted with CH_2Cl_2 (1.0 mL × 3). The organic phases were combined, dried over $MgSO_4$, filtered, and concentrated *in vacuo*. The crude product was purified on a silica gel column eluting with 10-40% EtOH/EtOAc to afford **18** as a white solid (120 mg, 30%). ^{1}H NMR (DMSO-d_6, 400 MHz): δ 8.35 (s, 2H), 7.72 (d, J = 1.8 Hz, 1H), 7.59 (dt, J = 8.0, 1.4 Hz, 1H), 7.47 (d, J = 7.8, 1.2 Hz, 1H), 7.38 (t, J = 7.8 Hz, 1H), 7.11 (d, J = 4.8 Hz, 1H), 4.51 (d, J = 16.1 Hz, 1H), 4.33 (d, J = 16.1 Hz, 1H), 3.70 (p, J = 8.3 Hz, 1H), 3.61 (t, J = 8.7 Hz, 1H), 3.20 (dd, J = 9.3, 7.3 Hz, 1H), 2.76 (dd, J = 16.4, 8.7 Hz, 1H), 2.50 (dd, overlap with DMSO solvent residue peak, 1H), 2.23 (s, 3H), 1.94 (m, 4H), 1.63 (m, 4H).

Ethyl 3-(3-bromophenyl)-4-nitrobutanoate (20): To a solution of compound **19** (5.00 mL, 31.2 mmol) in anhydrous THF (40.0 mL) under argon and cooled at 0 °C was added dropwise a solution of phosphorus ylide **9** (10.9 g, 31.23 mmol) in anhydrous CH_2Cl_2 (60.0 mL). The reaction mixture was stirred for 1 h at 5 °C, and then concentrated *in vacuo*. A mixture of hexanes and Et_2O (4:1, v/v, 40 mL) was added and the suspension was stirred for 10 min at ambient temperature. Filtration of the mixture through a silica gel plug and evaporation of the solvents afforded a white solid intermediate ethyl (Z)-3-(3-bromophenyl)acrylate (8.0 g, quantitative), which was used in the next step of synthesis without further purification. ^{1}H NMR ($CDCl_3$, 400 MHz): δ 7.65 (s, 1H), 7.58 (d, J = 16.0 Hz, 1H), 7.48 (dt, d, J = 7.9, 2.0 Hz, 1H), 7.42 (dt, d, J = 8.0, 1.4 Hz, 1H), 7.27-7.20 (m, 1H), 6.41 (d, J = 16.0 Hz, 1H), 4.25 (q, J = 7.1 Hz, 2H), 1.32 (t, J = 7.1 Hz, 3H).

The intermediate (8.0 g, 31.35 mmol) was dissolved in CH_3NO_2 (15 mL, 280 mmol) under argon and cooled at -20 °C. DBU (4.5 mL, 30.2 mmol) was added and the reaction mixture was kept stirring for 2 h at -20 °C. Water (10 mL) was added, followed by 12 N HCl until the pH of the mixture reached 1. The mixture was extracted with EtOAc (15 mL × 3). The combined organic phase was dried over Na_2SO_4 and concentrated *in vacuo*. The crude product compound **20** was obtained as a clear oil (9.5 g, quantitative) and used in the next step without further purification. ^{1}H NMR ($CDCl_3$, 400 MHz): δ 7.41 (dt, J = 7.7, 1.6 Hz, 1H), 7.36 (d, J = 1.9 Hz, 1H), 7.22-7.13 (m, 2H), 4.71 (dd, J = 12.8, 6.8 Hz, 1H), 4.61 (dd, J = 12.8, 8.0 Hz, 1H), 4.08 (q, J = 7.1 Hz, 2H), 3.94 (quint., J = 7.4 Hz, 1H), 2.72 (m, 2H), 1.17 (t, J = 7.1 Hz, 3H).

4-(3,-Bromophenyl)pyrrolidin-2-one (21): To a suspension of compound **20** (9.5 g, 30.2 mmol) and iron powder (17 g, 304.4 mmol) in a mixture of EtOH and water (2:1, v/v, 300 mL) was added NH_4Cl (55 g, 1,028 mmol). After stirring for 16 h at ambient temperature, the reaction mixture was adjusted to pH 14 with saturated NaOH solution and extracted with EtOAc (200 mL × 3). The combined organic phase was dried over Na_2SO_4 and concentrated *in vacuo* to afford compound **21** as a white solid (6.4 g, 88%), M.P. 95 - 97 °C. ^{1}H NMR ($CDCl_3$, 400 MHz): δ 7.39 (m, 2H), 7.23-7.14 (m, 2H), 5.82 (s, 1H), 3.77 (t, J = 8.2 Hz, 1H), 3.71-3.56 (m, 1H), 3.39 (m, 1H), 2.72 (dd, J = 16.9, 8.9 Hz, 1H), 2.45 (dd, J = 16.9, 8.6 Hz, 1H).

4-(3-Bromophenyl)-1-((3-methylpyridin-4-yl)methyl) pyrrolidin-2-one (22): To a solution of compound **21** (2 g, 8.3 mmol) in anhydrous THF (40 mL) under argon and cooled to 0 °C was added NaH (0.9 g, 22.5 mmol). TBAI (0.13 g, 0.35 mmol) and compound **12** (1.58 g, 8.87 mmol) were added after 30 min. The reaction mixture was kept stirring for 16 h at ambient temperature, then quenched with saturated $NaHCO_3$ solution (50 mL) and extracted with EtOAc (30 mL × 3). The combined organic phase was dried over Na_2SO_4 and concentrated *in vacuo*. The crude product was purified on a silica gel column eluting with 0-10% EtOH/EtOAc to afford compound **22** as a light brown oil (2.2 g, 76%). ^{1}H NMR ($CDCl_3$, 400 MHz): δ 8.40 (m, 2H), 7.38 (m, 1H), 7.31 (s, 1H), 7.18 (t, J = 7.8 Hz, 1H), 7.10 (dt, J = 7.7, 1.4 Hz, 1H), 7.02 (d, J = 5.0 Hz, 1H), 4.58 (d, J = 15.5 Hz, 1H), 4.42 (d, J = 15.5 Hz, 1H), 4.10 (q, J = 7.2 Hz, 1H), 3.65-3.58 (m, 1H), 3.28-3.17 (m, 1H), 2.96-2.82 (m, 1H), 2.61 (dd, J = 17.0, 8.1 Hz, 1H), 2.30 (s, 3H).

Chiral HPLC separation: Chiral separation of two enantiomers of **22** was done on a Chiralpak IA preparative column (10 × 250 mm, 5 μm), eluting with 100% MeOH. The enantiopurity was determined using a Chiralpak IA analytic column (4.6 × 250 mm)

eluting with 100% MeOH at flow rate of 1 mL/min, with the first peak (6.5 min) being (*S*)-**22** and second peak (9.0 min) being (*R*)-**22** (*ee*. > 99.8%). The enantiopure (*R*)-**22** was used in the next step.

***(R)*-1-((3-Methylpyridin-4-yl)methyl)-4-(3-(trimethylstannyl)phenyl)pyrrolidin-2-one (23):** To a solution of compound (*R*)-**22** (0.15 g, 0.43 mmol) in anhydrous toluene (1.5 mL) was added LiCl (0.11 g, 2.60 mmol), $Pd(PPh_3)_4$ (0.1 g, 0.09 mmol) and hexamethylditin (0.14 mL, 0.65 mmol) under argon. The reaction mixture was degassed with argon for 3 min and kept stirring at 105 °C for 1 h, then diluted with EtOAc (8 mL), passed through Celite and rinsed with EtOAc (4 mL × 2). The filtrate was concentrated *in vacuo*. The crude product was purified on a silica gel column eluting with 0-20% EtOH/EtOAc, followed by the trituration with $CHCl_3$ and hexane to afford the product **23** as a white solid (110 mg, 59%), M.P. 102-103 °C. ^{1}H NMR ($CDCl_3$, 400 MHz): δ 8.40-8.35 (m, 2H), 7.36 (dt, J = 7.2, 1.1 Hz, 1H), 7.31-7.23 (m, 2H), 7.13 (dt, J = 7.8, 1.7 Hz, 1H), 7.03 (d, J = 5.0 Hz, 1H), 4.60 (d, J = 15.6 Hz, 1H), 4.40 (d, J = 15.6 Hz, 1H), 3.65-3.53 (m, 2H), 3.28 (dd, J = 5.4, 2.4 Hz, 1H), 2.90 (dd, J = 17.0, 8.9 Hz, 1H), 2.67 (dd, J = 17.0, 8.4 Hz, 1H), 2.29 (s, 3H), 0.26 (s, 9H). ^{13}C NMR ($CDCl_3$, 100 MHz): δ 174.04, 151.14, 147.91, 143.37, 143.07, 141.24, 134.73, 134.26, 131.59, 128.48, 126.36, 122.22, 54.28, 43.58, 38.52, 37.31, 15.94, -9.51 (3C). HRMS: calculated for $C_{20}H_{26}N_2OSn$ ($[M + H]^+$) 431.1140; found, 431.1133.

Radiochemistry.

(*R*)-4-(3-(fluoro-^{18}F)phenyl)-1-((3-methylpyridin-4-yl)methyl)pyrrolidin-2-one ([^{18}F]7): Preparation from precursor **18**: The cyclotron produced aqueous [^{18}F]fluoride solution in ^{18}O-H_2O was transferred to a lead-shielded hot cell, where the [^{18}F]fluoride anion was trapped on a Chromafix® 30-PS-HCO_3 cartridge. The [^{18}F]fluoride was then eluted with a solution of tetraethyl ammonium bicarbonate (TEAB, 2 mg) in CH_3CN/water (7:3, v/v) into a reaction vessel. The solvent was azeotropically dried at 110 °C for 15 min, and dried further with anhydrous MeCN (1.0 mL × 2) at 110 °C. Then, a solution of about 2 mg of the radiolabeling precursor in 0.5 mL DMF was added. The reaction vessel was sealed, and heated at 150 °C for 10 min. The crude reaction mixture was diluted with HPLC mobile phase (1.5 mL) and purified by a reverse phase HPLC column [Luna C18(2), 10 µm, 100 Å, 10 × 250 mm]. The mobile phase was constituted with 25% CH_3CN and 75% ammonium formate solution (0.1 M, with 0.5 % AcOH, pH 4.2) at a flow rate of 5 mL/min. The eluent was monitored by a UV detector and a radioactivity detector. The fraction containing the racemic [^{18}F]**7** was collected, diluted with deionized (DI) water (50 mL), trapped on a C18 SepPak, washed with DI water (10 mL). The crude product was eluted off with ethanol (1 mL), diluted with DI water (1 mL), and loaded onto a ChiralCel OD-H column (10 × 250 mm, 5 µm) eluting with a mobile phase of 30% CH_3CN and 70% ammonium formate solution (0.1 M, with 0.5 % AcOH, pH 4.2) at a flow rate of 5 mL/min for separation of the two enantiomers. The fraction containing the (*R*)-enantiomer, [^{18}F]**7**, at 27.5 min, was collected (the other enantiomer eluted out at 24.2 min), diluted with DI water (50 mL), loaded on a C18 SepPak. The SepPak was washed with DI water (10 mL), and dried. The product was eluted off with EtOH (1 mL), diluted with USP grade saline (3 mL), passed through a sterile membrane filter (0.22 µm), and collected in a sterile vial pre-charged with 7 mL of USP saline and 20 µL of 8.4% $NaHCO_3$ solution to afford a formulated solution ready for administration.

Preparation from precursor **23**: [^{18}F]fluoride solution in ^{18}O-H_2O was trapped on a Chromafix cartridge pre-washed with EtOH (5 mL), an aqueous solution of potassium triflate (KOTf) (90 mg/mL, 5 mL) and DI water (5 mL). The potassium [^{18}F]fluoride was eluted off the cartridge into a 2 mL V-vial with an aqueous solution of KOTf (10 mg/mL, 0.45 mL) and K_2CO_3 (1 mg/mL, 50 µL), together with MeCN (0.5 mL). After three cycles of azeotropic trying as described above, a solution of the precursor **23** (2-3 mg) in anhydrous *N,N*-dimethylacetamide (DMA, 0.4 mL) was added to the reaction vial, followed by the solution of pyridine (1 M in DMA, 0.1 mL) and copper(II) triflate (0.2 M in DMA, 67 µL). The reaction mixture was agitated and then heated at 110° C for 20 min. The formulated [^{18}F]**7** solution was obtained following the purification and formulation protocol described above, without the use of chiral HPLC.

Measurement of lipophilicity. The log*D* of [^{18}F]**7** was determined by the modified method from previously published procedures[53]. Briefly, an aliquot of 0.74 MBq of the radioligand is added to a 2.0 mL microtube containing 0.8 mL 1-octanol and 0.8 mL 1X Dulbecco's phosphate buffered saline (1X D-PBS, pH 7.4). The mixture is subject to vigorous vortex for 20 s and centrifuged at 2,000 g for 2 min. A subsample of the octanol (0.2 mL) and 1X D-PBS (0.7 mL) layers was evaluated with a gamma counter. The major portion of the octanol layer (0.5 mL) was diluted with another 0.3 mL of octanol, mixed with a fresh portion of 0.8 mL PBS, vortexed, centrifuged, and analyzed as described above, till the log*D* value stabilized.

Measurement of Plasma Free Fraction (f_p). The unbound fraction of [^{18}F]**7** in the plasma (f_p) was measured in triplicate using the ultrafiltration method[24]. Briefly, [^{18}F]**7** (5.55 MBq, 0.1 mL) was added to 3.0 mL of whole nonhuman primate blood. After 10 min incubation at ambient temperature, the blood sample was centrifuged at 2,930 g for 5 min. The supernatant plasma (0.3 mL) was loaded onto the reservoir of a micropartition device (MilliporeSigma Centrifree Ultrafiltration, Burlington, MA) in triplicate and centrifuged at 1,228 g for 20 min. The f_p value was calculated as the ratio of radioactivity in the filtrate to that in the plasma.

Nonhuman Primate PET Imaging. The study in this project was performed under a protocol approved by the Yale University Institutional Animal Care and Use Committee (IACUC). Rhesus monkeys (*Macaca mulatta*) were fasted overnight prior to the imaging study. The animals were sedated using intramuscular (*i.m.*) injection of ketamine and glycopyrrolate approximately 2 h before the PET scan, and anesthesia was subsequently maintained with isoflurane (1.5%–2.5%) for the duration of the imaging experiments. A water-jacket heating pad was used to maintain body temperature. The animal was attached to a physiological monitor, and vital signs (pulse rate, blood pressure, respirations, EKG, ETCO2 and body temperature) were continuously monitored. After a transmission scan, the radioligand was injected *i.v.* as a 3 min slow bolus by an infusion pump (PHD 22/2000; Harvard Apparatus). Dynamic PET scans were performed for two hours with a Focus-220 PET scanner (Siemens Preclinical Solutions) with a reconstructed image resolution of approximately 1.5 mm. Arterial blood samples were collected during the PET scans to measure the radioactivity in plasma for generation of the metabolite-corrected arterial plasma input function. PET images were reconstructed with built-in corrections for attenuation, normalization, scatter, randoms, and deadtime. PET images were registered to the animal's MR image, which was subsequently registered to a brain atlas to define the regions-of-interest.

Plasma Radiometabolite Analysis. Plasma radiometabolite analysis was performed using the column switching method, following published protocol[54]. Briefly, arterial blood samples were collected at 5, 15, 30, 60, and 90 min *p.i.*, treated with urea (8 M), filtered, trapped on a capture column (4.6 × 19 mm), back flashed to a Phenomenex Luna C18(2) column (5 μm, 4.6 × 250 mm), eluted with 37% acetonitrile/63% 0.1 M ammonium formate (pH 6.4) at flow rate of 2 mL/min, and analyzed by radio-HPLC to determine the fraction of intact [^{18}F]**7** in the plasma.

Kinetic Modeling. A rhesus monkey brain atlas was used for generation of regions-of-interest (ROIs) and time-activity curves (TACs). Volume of distribution (V_T, mL·cm^{-3}) values were derived through 1-tissue (1T) compartment kinetic modeling with the metabolite-corrected arterial plasma input function, which was calculated as the product of the fitted total plasma curve and the parent radiotracer fraction curve. Non-displaceable binding potential (BP_{ND}) values were calculated from V_T values using centrum semiovale (CS) as reference region, *i.e.*, $BP_{ND} = (V_{T\ ROI} - V_{T\ CS})/V_{T\ CS}$. Specific binding of the radioligands to SV2A was evaluated by one pre-blocking study with unlabeled UCB-J (150 μg/kg, *i.v.*, given 10 min before tracer injection, as used in previous studies[19]) in one of the three rhesus monkeys. SV2A occupancy by UCB-J was calculated using the Lassen plot[55]. For time stability of V_T estimates (1TCM) of [^{18}F]**7**, **4**, and **6**, the V_T estimates of 17 brain regions (amygdala, brainstem, caudate, cerebellum, cingulate cortex, frontal cortex, globus pallidus, hippocampus, insula, nucleus accumbens, occipital, pons, putamen, centrum semiovale, substantia nigra, temporal cortex, and thalamus) were generated using scan durations ranging from 30 to 120 min in 15 min increments. The V_T estimates were normalized by V_T estimates using 120 min scan duration. Within 10% deviation of the averaged V_T estimates from V_T estimates using 120 min scan duration was considered acceptable.

ASSOCIATED CONTENT

Supporting Information

NMR spectra of compounds **7**, **10, 11, 14, 15, 16, 18, 20, 21, 22,** and **23.** HPLC profiles of **7** and **22**, table of quality control results, and table of radiosynthesis results of [^{18}F]**7**. This material is available free of charge via the Internet at http://pubs.acs.org.

AUTHOR INFORMATION

Corresponding Author

*E-mail: jason.cai@yale.edu; songye.li@yale.edu; Fax: +1-(203)785-2994; Tel: +1-(203)785-7691.

Author Contributions

Z.C., S.L. contributed equally. Z.C., S.L., R.P., W.Z., X.W., E.B., D.H, S.J.F., D.L., J.R., and N.B.N. performed the experiments. Z.C., S.L., R.E.C., and Y.H. designed the experiments. Z.C. wrote the first draft of the manuscript. All authors contributed to and approved the final version of the manuscript.

Funding

This research was supported by NIH K01EB023312, R01AG058773, and R01AG052560. Z.C. is an Archer Foundation Research Scientist.

Notes

The authors declare no competing financial interest.

#Current address: Department of Nuclear Medicine, West China Hospital, Sichuan University, Chengdu, China.
&Current address: Brown University, Providence, RI. USA.
ˊCurrent address: AbbVie, Chicago, IL. USA.

ACKNOWLEDGMENT

The authors thank Yale PET center staff for the production of ^{18}F and the expert support of nonhuman primate PET imaging.

REFERENCES

1. Bajjalieh, S.; Peterson, K.; Shinghal, R.; Scheller, R., SV2, a brain synaptic vesicle protein homologous to bacterial transporters. *Science* **1992,** *257* (5074), 1271-1273.
2. Crowder, K. M.; Gunther, J. M.; Jones, T. A.; Hale, B. D.; Zhang, H. Z.; Peterson, M. R.; Scheller, R. H.; Chavkin, C.; Bajjalieh, S. M., Abnormal neurotransmission in mice lacking synaptic vesicle protein 2A (SV2A). *Proc. Natl. Acad. Sci. U.S.A.* **1999,** *96* (26), 15268-15273.
3. Mendoza-Torreblanca, J. G.; Vanoye-Carlo, A.; Phillips-Farfán, B. V.; Carmona-Aparicio, L.; Gómez-Lira, G., Synaptic vesicle protein 2A: basic facts and role in synaptic function. *Eur. J. Neurosci.* **2013,** *38* (11), 3529-3539.
4. Feng, G.; Xiao, F.; Lu, Y.; Huang, Z.; Yuan, J.; Xiao, Z.; Xi, Z.; Wang, X., Down-regulation synaptic vesicle protein 2A in the anterior temporal neocortex of patients with intractable epilepsy. *J. Mol. Neurosci.* **2009,** *39* (3), 354-359.
5. Loscher, W.; Gillard, M.; Sands, Z. A.; Kaminski, R. M.; Klitgaard, H., Synaptic Vesicle Glycoprotein 2A Ligands in the Treatment of Epilepsy and Beyond. *CNS Drugs* **2016,** *30* (11), 1055-1077.
6. Tokudome, K.; Okumura, T.; Shimizu, S.; Mashimo, T.; Takizawa, A.; Serikawa, T.; Terada, R.; Ishihara, S.; Kunisawa, N.; Sasa, M.; Ohno, Y., Synaptic vesicle glycoprotein 2A (SV2A) regulates kindling epileptogenesis via GABAergic neurotransmission. *Sci. Rep.* **2016,** *6*, 27420.
7. Sanchez, P. E.; Zhu, L.; Verret, L.; Vossel, K. A.; Orr, A. G.; Cirrito, J. R.; Devidze, N.; Ho, K.; Yu, G. Q.; Palop, J. J.; Mucke, L., Levetiracetam suppresses neuronal network dysfunction and reverses synaptic and cognitive deficits in an Alzheimer's disease model. *Proc. Natl. Acad. Sci. U.S.A.* **2012,** *109* (42), E2895-903.
8. Lynch, B. A.; Lambeng, N.; Nocka, K.; Kensel-Hammes, P.; Bajjalieh, S. M.; Matagne, A.; Fuks, B., The synaptic vesicle protein SV2A is the binding site for the antiepileptic drug levetiracetam. *Proc. Natl. Acad. Sci. U.S.A.* **2004,** *101* (20), 9861-9866.
9. Bakker, A.; Krauss, Gregory L.; Albert, Marilyn S.; Speck, Caroline L.; Jones, Lauren R.; Stark, Craig E.; Yassa, Michael A.; Bassett, Susan S.; Shelton, Amy L.; Gallagher, M., Reduction of Hippocampal Hyperactivity Improves Cognition in Amnestic Mild Cognitive Impairment. *Neuron* **2012,** *74* (3), 467-474.
10. Koh, M. T.; Haberman, R. P.; Foti, S.; McCown, T. J.; Gallagher, M., Treatment Strategies Targeting Excess Hippocampal Activity Benefit Aged Rats with Cognitive Impairment. *Neuropsychopharmacology* **2010,** *35* (4), 1016-1025.
11. Stockburger, C. M., Davide; Baeumlisberger, Marion; Pallas, Thea; Arrey, Tabiwang N.; Karas, Michael; Friedland, Kristinad; Müller, Walter E., A Mitochondrial Role of SV2a Protein in Aging and Alzheimer's Disease: Studies with Levetiracetam. *J. Alzheimer's Dis.* **2016,** *50* (1), 201-215.
12. Cai, Z.; Li, S.; Matuskey, D.; Nabulsi, N.; Huang, Y., PET imaging of synaptic density: A new tool for investigation of neuropsychiatric diseases. *Neurosci. Lett.* **2019,** *691*, 44-50.
13. Cai, H.; Mangner, T. J.; Muzik, O.; Wang, M.-W.; Chugani, D. C.; Chugani, H. T., Radiosynthesis of ^{11}C-Levetiracetam: A Potential Marker for PET Imaging of SV2A Expression. *ACS Med. Chem. Lett.* **2014,** *5* (10), 1152-1155.
14. Estrada, S.; Lubberink, M.; Thibblin, A.; Sprycha, M.; Buchanan, T.; Mestdagh, N.; Kenda, B.; Mercier, J.; Provins, L.; Gillard, M.; Tytgat, D.; Antoni, G., [^{11}C]UCB-A, a novel PET tracer for synaptic vesicle protein 2 A. *Nucl. Med. Biol.* **2016,** *43* (6), 325-332.
15. Warnock, G. I.; Aerts, J.; Bahri, M. A.; Bretin, F.; Lemaire, C.; Giacomelli, F.; Mievis, F.; Mestdagh, N.; Buchanan, T.; Valade, A.; Mercier, J.; Wood, M.; Gillard, M.; Seret, A.;

Luxen, A.; Salmon, E.; Plenevaux, A., Evaluation of ^{18}F-UCB-H as a novel PET tracer for synaptic vesicle protein 2A in the brain. *J. Nucl. Med.* **2014,** *55* (8), 1336-41.
16. Bretin, F.; Bahri, M. A.; Bernard, C.; Warnock, G.; Aerts, J.; Mestdagh, N.; Buchanan, T.; Otoul, C.; Koestler, F.; Mievis, F.; Giacomelli, F.; Degueldre, C.; Hustinx, R.; Luxen, A.; Seret, A.; Plenevaux, A.; Salmon, E., Biodistribution and Radiation Dosimetry for the Novel SV2A Radiotracer [^{18}F]UCB-H: First-in-Human Study. *Mol. Imag. Biol.* **2015,** *17* (4), 557-564.
17. Bahri, M. A.; Plenevaux, A.; Aerts, J.; Bastin, C.; Becker, G.; Mercier, J.; Valade, A.; Buchanan, T.; Mestdagh, N.; Ledoux, D.; Seret, A.; Luxen, A.; Salmon, E., Measuring brain synaptic vesicle protein 2A with positron emission tomography and [^{18}F]UCB-H. *Alzheimers Dement. (N Y)* **2017,** *3* (4), 481-486.
18. Becker, G.; Warnier, C.; Serrano, M. E.; Bahri, M. A.; Mercier, J.; Lemaire, C.; Salmon, E.; Luxen, A.; Plenevaux, A., Pharmacokinetic Characterization of [^{18}F]UCB-H PET Radiopharmaceutical in the Rat Brain. *Mol Pharm* **2017,** *14* (8), 2719-2725.
19. Nabulsi, N.; Mercier, J.; Holden, D.; Carre, S.; Najafzadeh, S.; Vandergeten, M.-C.; Lin, S.-f.; Deo, A. K.; Price, N.; Wood, M.; Lara-Jaime, T.; Montel, F.; Laruelle, M.; Carson, R. E.; Hannestad, J.; Huang, Y., Synthesis and Preclinical Evaluation of ^{11}C-UCB-J as a PET Tracer for Imaging the Synaptic Vesicle Glycoprotein 2A in the Brain. *J. Nucl. Med.* **2016**, *57*(5), 777-784.
20. Finnema, S. J.; Nabulsi, N. B.; Eid, T.; Detyniecki, K.; Lin, S. F.; Chen, M. K.; Dhaher, R.; Matuskey, D.; Baum, E.; Holden, D.; Spencer, D. D.; Mercier, J.; Hannestad, J.; Huang, Y.; Carson, R. E., Imaging synaptic density in the living human brain. *Sci. Transl. Med.* **2016,** *8* (348), 348ra96.
21. Finnema, S. J.; Nabulsi, N. B.; Mercier, J.; Lin, S. F.; Chen, M. K.; Matuskey, D.; Gallezot, J. D.; Henry, S.; Hannestad, J.; Huang, Y.; Carson, R. E., Kinetic evaluation and test-retest reproducibility of [^{11}C]UCB-J, a novel radioligand for positron emission tomography imaging of synaptic vesicle glycoprotein 2A in humans. *J. Cereb. Blood Flow Metab.* **2018,** *38* (11), 2041-2052.
22. Chen, M. K.; Mecca, A. P.; Naganawa, M.; Finnema, S. J.; Toyonaga, T.; Lin, S. F.; Najafzadeh, S.; Ropchan, J.; Lu, Y.; McDonald, J. W.; Michalak, H. R.; Nabulsi, N. B.; Arnsten, A. F. T.; Huang, Y.; Carson, R. E.; van Dyck, C. H., Assessing Synaptic Density in Alzheimer Disease With Synaptic Vesicle Glycoprotein 2A Positron Emission Tomographic Imaging. *JAMA Neurol.* **2018**, *75*(10), 1215-1224.
23. Li, S.; Cai, Z.; Zhang, W.; Nabulsi, N.; Finnema, S.; Holden, D.; Ropchan, J.; Gao, H.; Teng, J.-K.; Carson, R.; Huang, Y., Synthesis and in vivo evaluation of ^{18}F-UCB-J: Radiotracer for PET imaging of synaptic density. *J. Nucl. Med.* **2017,** *58* (supplement 1), S851.
24. Li, S.; Cai, Z.; Wu, X.; Holden, D.; Pracitto, R.; Kapinos, M.; Gao, H.; Labaree, D.; Nabulsi, N.; Carson, R. E.; Huang, Y., Synthesis and in Vivo Evaluation of a Novel PET Radiotracer for Imaging of Synaptic Vesicle Glycoprotein 2A (SV2A) in Nonhuman Primates. *ACS Chem. Neurosci.* **2019,** *10* (3), 1544-1554.
25. Constantinescu, C. C.; Tresse, C.; Zheng, M.; Gouasmat, A.; Carroll, V. M.; Mistico, L.; Alagille, D.; Sandiego, C. M.; Papin, C.; Marek, K.; Seibyl, J. P.; Tamagnan, G. D.; Barret, O., Development and In Vivo Preclinical Imaging of Fluorine-18-Labeled Synaptic Vesicle Protein 2A (SV2A) PET Tracers. *Mol. Imag. Biol.* **2018**, *21* (3), 509-518.
26. Heurling, K.; Ashton, N. J.; Leuzy, A.; Zimmer, E. R.; Blennow, K.; Zetterberg, H.; Eriksson, J.; Lubberink, M.; Schöll, M., Synaptic vesicle protein 2A as a potential biomarker in synaptopathies. *Mol. Cell. Neurosci.* **2019**, *97*, 34-42.
27. Toyonaga, T.; Smith, L. M.; Finnema, S. J.; Gallezot, J.-D.; Naganawa, M.; Bini, J.; Mulnix, T.; Cai, Z.; Ropchan, J.; Huang, Y.; Strittmatter, S. M.; Carson, R. E., In vivo synaptic density imaging with ^{11}C-UCB-J detects treatment effects of saracatinib (AZD0530) in a mouse model of Alzheimer's disease. *J. Nucl. Med.* **2019**, *60* (12), 1780-1786.
28. Holmes, S. E.; Scheinost, D.; Finnema, S. J.; Naganawa, M.; Davis, M. T.; DellaGioia, N.; Nabulsi, N.; Matuskey, D.; Angarita, G. A.; Pietrzak, R. H.; Duman, R. S.; Sanacora, G.; Krystal, J. H.; Carson, R. E.; Esterlis, I., Lower synaptic density is associated with depression severity and network alterations. *Nat. Commun.* **2019,** *10* (1), 1529.
29. Li, S.; Cai, Z.; Zhang, W.; Holden, D.; Lin, S.-f.; Finnema, S. J.; Shirali, A.; Ropchan, J.; Carre, S.; Mercier, J.; Carson, R. E.; Nabulsi, N.; Huang, Y., Synthesis and in vivo evaluation of [^{18}F]UCB-J for PET imaging of synaptic vesicle glycoprotein 2A (SV2A). *Eur. J. Nucl. Med. Mol. Imaging* **2019,** *46* (9), 1952-1965.
30. Tredwell, M.; Preshlock, S. M.; Taylor, N. J.; Gruber, S.; Huiban, M.; Passchier, J.; Mercier, J.; Genicot, C.; Gouverneur, V., A general copper-mediated nucleophilic ^{18}F fluorination of arenes. *Angew. Chem. Int. Ed. Engl.* **2014,** *53* (30), 7751-5.
31. Mossine, A. V.; Brooks, A. F.; Makaravage, K. J.; Miller, J. M.; Ichiishi, N.; Sanford, M. S.; Scott, P. J. H., Synthesis of [^{18}F]Arenes via the Copper-Mediated [^{18}F]Fluorination of Boronic Acids. *Org. Lett.* **2015,** *17* (23), 5780-5783.
32. Pike, V. W.; Aigbirhio, F. I., Reactions of cyclotron-produced [^{18}F]fluoride with diaryliodonium salts-a novel single-step route to no-carrier-added [^{18}]fluoroarenes. *J. Chem. Soc., Chem. Commun.* **1995,** *21*, 2215-2216.
33. Zhang, M.-R.; Kumata, K.; Suzuki, K., A practical route for synthesizing a PET ligand containing [^{18}F]fluorobenzene using reaction of diphenyliodonium salt with [^{18}F]F−. *Tetrahedron Lett.* **2007,** *48* (49), 8632-8635.
34. Rotstein, B. H.; Stephenson, N. A.; Vasdev, N.; Liang, S. H., Spirocyclic hypervalent iodine(III)-mediated radiofluorination of non-activated and hindered aromatics. *Nat. Commun.* **2014,** *5*, 4365.
35. Sander, K.; Gendron, T.; Yiannaki, E.; Cybulska, K.; Kalber, T. L.; Lythgoe, M. F.; Arstad, E., Sulfonium Salts as Leaving Groups for Aromatic Labelling of Drug-like Small Molecules with Fluorine-18. *Sci. Rep.* **2015,** *5*, 9941.
36. Makaravage, K. J.; Brooks, A. F.; Mossine, A. V.; Sanford, M. S.; Scott, P. J. H., Copper-Mediated Radiofluorination of Arylstannanes with [18F]KF. *Org. Lett.* **2016,** *18* (20), 5440-5443.
37. Campbell, M. G.; Ritter, T., Late-Stage Fluorination: From Fundamentals to Application. *Org. Process Res. Dev.* **2014,** *18* (4), 474-480.
38. Li, S.; Cai, Z.; Holden, D.; Nabulsi, N.; Labaree, D.; Shirali, A.; Teng, J.-k.; Carson, R.; Huang, Y., ^{18}F-SDM-8: A novel radiotracer for PET imaging of synaptic density. *J. Nucl. Med.* **2018,** *59* (supplement 1), S68.
39. Cai, Z.; Li, S.; Finnema, S.; Lin, S.-f.; Zhang, W.; Holden, D.; Carson, R.; Huang, Y., Imaging synaptic density with novel ^{18}F-labeled radioligands for synaptic vesicle protein-2A (SV2A): synthesis and evaluation in nonhuman primates. *J. Nucl. Med.* **2017,** *58* (supplement 1), S547.
40. Patel, S.; Knight, A.; Krause, S.; Teceno, T.; Tresse, C.; Li, S.; Cai, Z.; Gouasmat, A.; Carroll, V. M.; Barret, O.; Gottmukkala, V.; Zhang, W.; Xiang, X.; Morley, T.; Huang, Y.; Passchier, J., Preclinical In Vitro and In Vivo Characterization of Synaptic Vesicle 2A–Targeting

Compounds Amenable to F-18 Labeling as Potential PET Radioligands for Imaging of Synapse Integrity. *Mol. Imaging Biol.* [Online early access]. DOI: 10.1007/s11307-019-01428-0. Published online: Nov 14, 2019.
41. Gillard, M.; Fuks, B.; Michel, P.; Vertongen, P.; Massingham, R.; Chatelain, P., Binding characteristics of [^{3}H]ucb 30889 to levetiracetam binding sites in rat brain. *Eur. J. Pharmacol.* **2003,** *478* (1), 1-9.
42. Gillard, M.; Chatelain, P.; Fuks, B., Binding characteristics of levetiracetam to synaptic vesicle protein 2A (SV2A) in human brain and in CHO cells expressing the human recombinant protein. *Eur. J. Pharmacol.* **2006,** *536* (1–2), 102-108.
43. Brooks, A. F.; Topczewski, J. J.; Ichiishi, N.; Sanford, M. S.; Scott, P. J. H., Late-stage [^{18}F]fluorination: new solutions to old problems. *Chem. Sci.* **2014,** *5* (12), 4545-4553.
44. Cardinale, J.; Ermert, J.; Humpert, S.; Coenen, H. H., Iodonium ylides for one-step, no-carrier-added radiofluorination of electron rich arenes, exemplified with 4-(([^{18}F]fluorophenoxy)-phenylmethyl)piperidine NET and SERT ligands. *RSC Advances* **2014,** *4* (33), 17293-17299.
45. Wang, L.; Jacobson, O.; Avdic, D.; Rotstein, B. H.; Weiss, I. D.; Collier, L.; Chen, X.; Vasdev, N.; Liang, S. H., Ortho-Stabilized ^{18}F-Azido Click Agents and their Application in PET Imaging with Single-Stranded DNA Aptamers. *Angew. Chem. Int. Ed.* **2015,** *54* (43), 12777-12781.
46. Stephenson, N. A.; Holland, J. P.; Kassenbrock, A.; Yokell, D. L.; Livni, E.; Liang, S. H.; Vasdev, N., Iodonium Ylide–Mediated Radiofluorination of ^{18}F-FPEB and Validation for Human Use. *J. Nucl. Med.* **2015,** *56* (3), 489-492.
47. Jacobson, O.; Weiss, I. D.; Wang, L.; Wang, Z.; Yang, X.; Dewhurst, A.; Ma, Y.; Zhu, G.; Niu, G.; Kiesewetter, D. O.; Vasdev, N.; Liang, S. H.; Chen, X., ^{18}F-Labeled Single-Stranded DNA Aptamer for PET Imaging of Protein Tyrosine Kinase-7 Expression. *J. Nucl. Med.* **2015,** *56* (11), 1780-1785.
48. Rotstein, B. H.; Wang, L.; Liu, R. Y.; Patteson, J.; Kwan, E. E.; Vasdev, N.; Liang, S. H., Mechanistic studies and radiofluorination of structurally diverse pharmaceuticals with spirocyclic iodonium(iii) ylides. *Chem. Sci.* **2016,** *7* (7), 4407-4417.
49. Pajouhesh, H.; Lenz, G. R., Medicinal chemical properties of successful central nervous system drugs. *NeuroRx* **2005,** *2* (4), 541-553.
50. Rossano, S.; Toyonaga, T.; Finnema, S. J.; Naganawa, M.; Lu, Y.; Nabulsi, N.; Ropchan, J.; De Bruyn, S.; Otoul, C.; Stockis, A.; Nicolas, J. M.; Martin, P.; Mercier, J.; Huang, Y.; Maguire, R. P.; Carson, R. E., Assessment of a white matter reference region for ^{11}C-UCB-J PET quantification. *J. Cereb. Blood Flow Metab.* [Online early access]. DOI: 10.1177/0271678X19879230. Published online: Sep 30, 2019.
51. Mertens, N.; Maguire, R. P.; Serdons, K.; Lacroix, B.; Mercier, J.; Sciberras, D.; Van Laere, K.; Koole, M., Validation of Parametric Methods for [^{11}C]UCB-J PET Imaging Using Subcortical White Matter as Reference Tissue. *Mol. Imag. Biol.* [Online early access]. DOI: 10.1007/s11307-019-01387-6. Published online: Jun 17, 2019.
52. Koole, M.; van Aalst, J.; Devrome, M.; Mertens, N.; Serdons, K.; Lacroix, B.; Mercier, J.; Sciberras, D.; Maguire, P.; Van Laere, K., Quantifying SV2A density and drug occupancy in the human brain using [^{11}C]UCB-J PET imaging and subcortical white matter as reference tissue. *Eur. J. Nucl. Med. Mol. Imag.* **2019,** *46* (2), 396-406.
53. Wilson, A. A.; Jin, L.; Garcia, A.; DaSilva, J. N.; Houle, S., An admonition when measuring the lipophilicity of radiotracers using counting techniques. *Appl. Radiat. Isot.* **2001,** *54* (2), 203-208.
54. Hilton, J.; Yokoi, F.; Dannals, R. F.; Ravert, H. T.; Szabo, Z.; Wong, D. F., Column-switching HPLC for the analysis of plasma in PET imaging studies. *Nucl. Med. Biol.* **2000,** *27* (6), 627-630.
55. Cunningham, V. J.; Rabiner, E. A.; Slifstein, M.; Laruelle, M.; Gunn, R. N., Measuring drug occupancy in the absence of a reference region: the Lassen plot re-visited. *J. Cereb. Blood Flow Metab.* **2010,** *30* (1), 46-50.

Table of Contents artwork

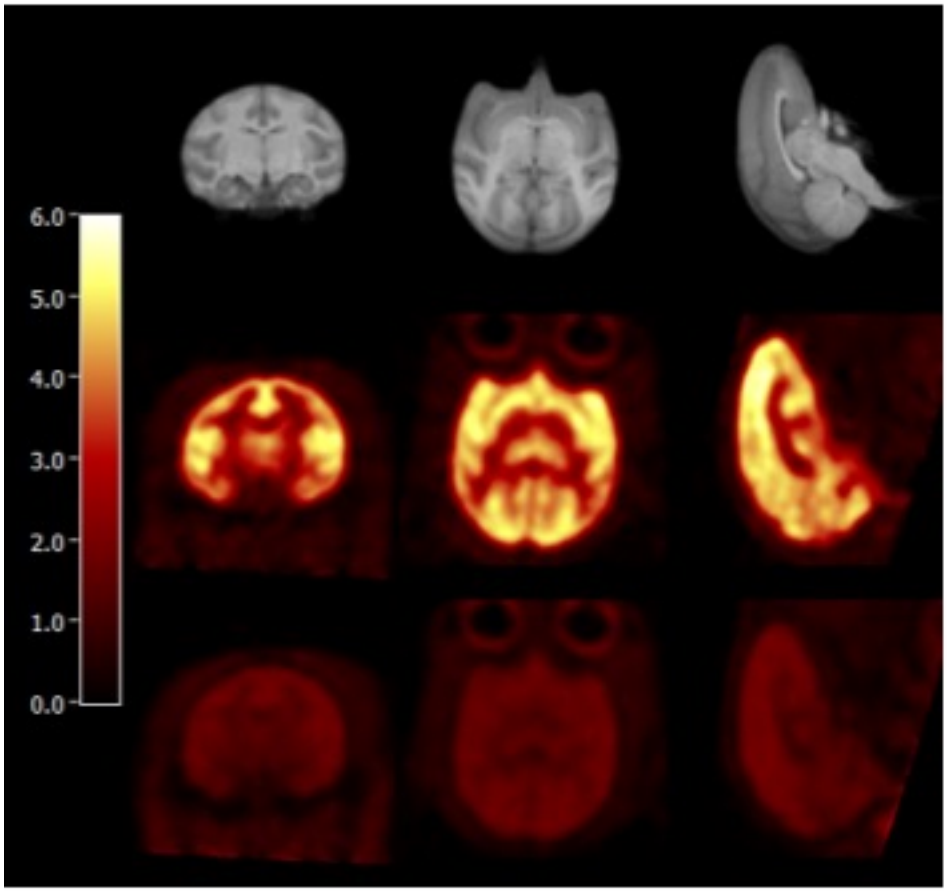
6.0
5.0
4.0
3.0
2.0
1.0
0.0

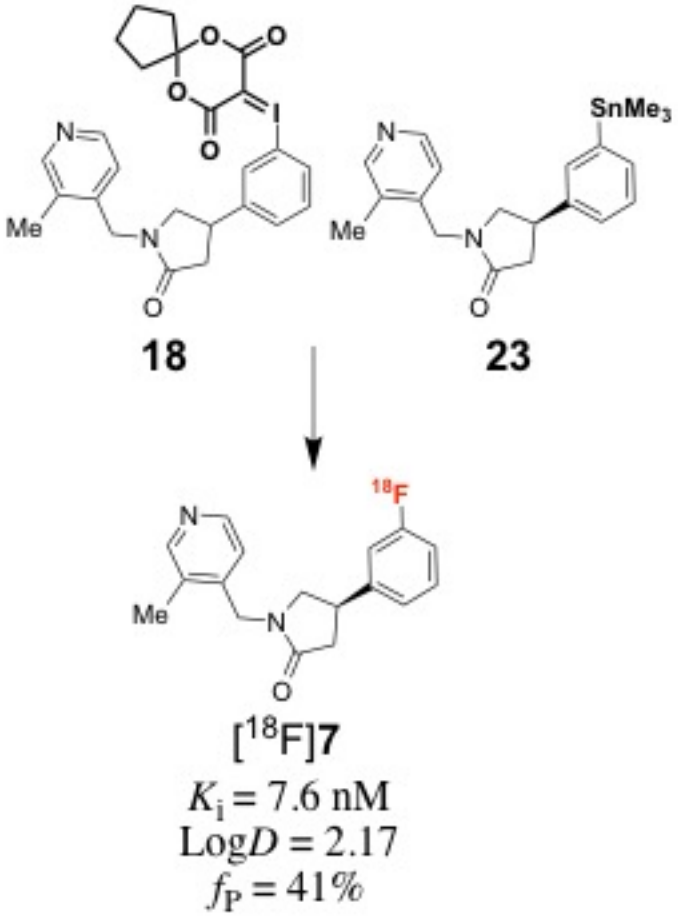
Me
N
O
I
SnMe3
18
23
18F
[18F]7
Ki = 7.6 nM
LogD = 2.17
fP = 41%